Membrane and Water Treatment, *Vol. 12, No. 5 (2021) 205-216*
https://doi.org/10.12989/mwt.2021.12.5.205

fMWNTs/GO/MnO_2 nanocomposites as additives in a membrane for the removal of crystal violet

Sabna V*[1], Santosh G Thampi[1a], S Chandrakaran[1a], Sasina E P[2b] and Resmi P[2b]

[1]*Department of Civil Engineering, National Institute of Technology Calicut, Kozhikode, Kerala, India-673 601*
[2]*Department of Environmental Science, University of Calicut, Kerala, India-673 635*

(Received February 23, 2019, Revised May 31, 2021, Accepted May 31, 2021)

Abstract. In this work, the performance of a mixed matrix membrane in the removal of crystal violet from aqueous solutions is reported. This membrane was fabricated by adding a nanocomposite (fMWNTs/GO/MnO_2 NC) synthesized with functionalized multi-walled carbon nanotubes, graphene oxide, and manganese dioxide nanoparticles, to polysulfone. Details pertaining to the preparation and characterization of the membrane, evaluation of its performance in the removal of crystal violet, and antifouling properties of the membrane are reported in this paper. The membranes were fabricated by embedding varying concentrations of fMWNTs/GO/MnO_2 NC (from 0 to 0.3wt%) in the Psf matrix. Incorporation of fMWNTs/GO/MnO2 NC was found to enhance hydrophilicity, equilibrium water content, porosity, mean pore radius, pure water permeability and antifouling properties of the membrane. Analyses of surface morphology of the fabricated membranes revealed the presence of macro-voids in the matrix of the membrane after addition of fMWNTs/GO/MnO_2 NC, resulting in an increase in pure water flux and permeability. It was observed that 0.1wt% is the optimum concentration of fMWNTs/GO/MnO2 NC in the Psf matrix since the membrane exhibited maximum hydrophilicity, equilibrium water content, porosity, pure water permeability and dye rejection at this concentration. Also, it was observed that the polysulfone membrane exhibited enhanced antifouling properties at this concentration of the nanocomposite.

Keywords: antifouling; crystal violet; membrane filtration; nanocomposite

1. Introduction

Scarcity of fresh water is a serious problem in many regions around the world. Reliable and sustainable supplies of good quality water are vital for domestic consumption, agriculture, industry, recreation, and energy generation. Continued population growth, contamination of both surface and ground waters, uneven distribution of water resources and periodic droughts have forced water utilities to search for alternate sources of water supply. Wastewater reuse has drawn increasing attention worldwide as an integral part of water resources management. Reuse and recovery of municipal and industrial wastewaters can be achieved by adopting appropriate wastewater treatment processes (Wang and Tarabara 2007). Technologies like adsorption, catalytic degradation, advanced membrane filtration, chemical treatment, fixed-media devices, enhanced air flotation etc. are being used to recycle water economically and to achieve zero liquid discharge. Membrane processes involve separation of two components in a mixture using a semi-permeable membrane made of inorganic or organic polymer materials. This can be used for gas separation, liquid separation, separation of solids from liquids etc. Processes employed include membrane distillation (Gryta 2010), membrane electro dialysis (Tanaka 2010), and membrane filtration (Nandhi *et al*. 2011, Morao *et al*. 2011).

Membranes are thin and porous sheets of material that separate contaminants from water when a driving force is applied. Based on the size of the pores in the membrane and the operating pressure, membrane processes can be divided into four types, viz. microfiltration (MF), ultrafiltration (UF), nanofiltration (NF), and reverse osmosis (RO). Membranes are fabricated in four main types of modules: plate-and-frame, tubular, spiral wound, and hollow fibre. Two types of modules are generally used for evaluating the performance of membranes. These are dead end cell and cross flow cell (Fig. 1). In membrane processes, steric hindrance and electrostatic repulsion cause the separation of solutes from aqueous solutions.

Organic membranes are fabricated by phase inversion mechanism, using three components, namely, a polymer, a solvent and a non-solvent (Fig. 2). Dry phase inversion and wet phase inversion are the two variations of the phase inversion process. Wet phase inversion process is generally used for the fabrication of membranes (Vatanpour *et al*. 2011, Ladan *et al*. 2014).

Polysulfone, polyethersulfone, and polyvinyl fluoride are generally used as host polymer materials in the fabrication of mixed matrix membranes. These materials are widely used for the synthesis of MF, UF, NF and RO membranes due to its chemical and thermal resistance, tolerance to variation in pH, easy processing, environmental

*Corresponding author, Ph.D.,
E-mail: sabnavv@gmail.com
[a] Professor
[b] Student

ISSN: 2005-8624 (Print), 2092-7037 (Online)

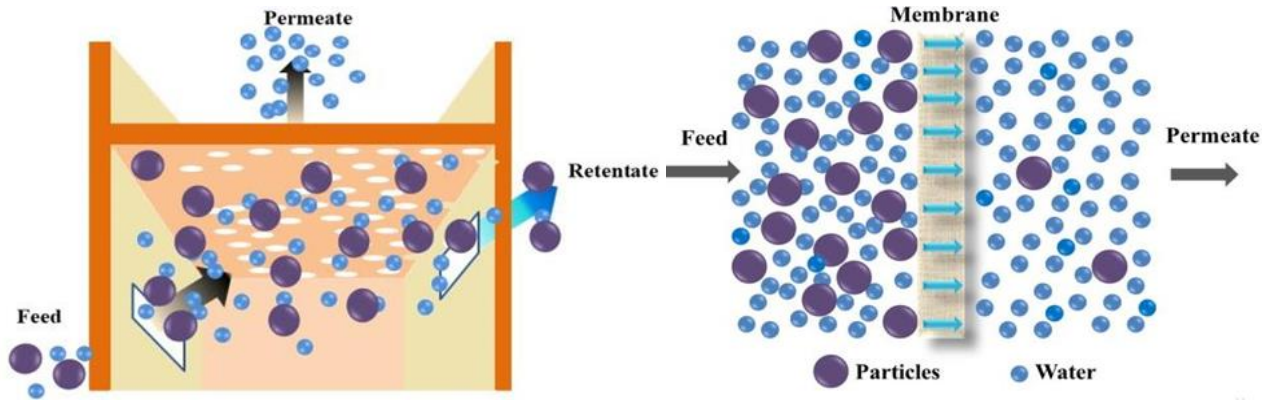

Fig. 1 Schematic representation of cross flow membrane filtration process

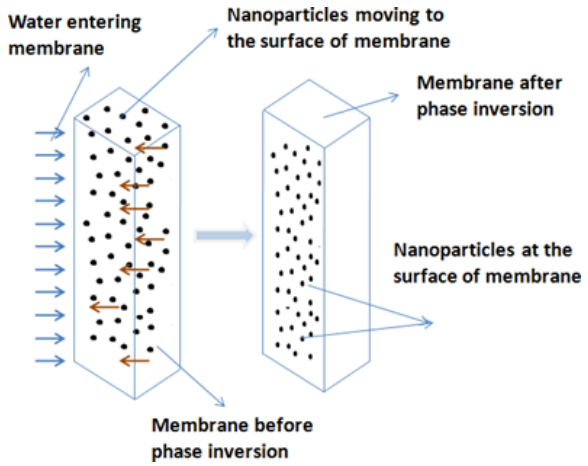

Fig. 2 Phase inversion mechanism

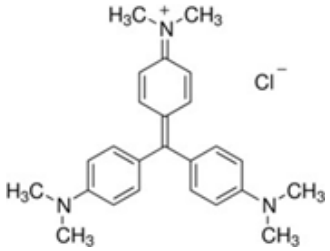

Fig. 3 Structure of crystal violet

endurance, and broad pore size range.

N-methyl pyrrolidone, dimethyl sulfone etc. are some of the solvents used in membrane fabrication to dissolve the polymer material and make the membrane casting solution. Non-solvents like water are used for coagulation of the polymer, leading to the formation of membranes. Achieving maximum permeate flow and maximum solute rejection with minimum capital and operating costs are the criteria employed for optimising the design of membrane processes (Sablani *et al*. 2001, Maskan *et al*. 2000). It is desirable to have a membrane with as long a life span as possible (Sablani *et al*. 2001). Membrane fouling caused by microbial adhesion, gel layer formation, solute adhesion, and concentration polarisation due to solute build-up at the membrane surface are the primary factors that affect the lifespan and permeate flux of membranes (Maskan *et al*. 2000). Improvement in the hydrophilicity of polymer membranes reduces biofouling because protein-like foulants are hydrophobic in nature. Surface modification of the membranes has been widely employed to improve the permeation properties of hydrophobic membranes and to reduce the adsorption of proteins (Higuchi *et al*. 2010). This is achieved by incorporating hydrophilic inorganic materials into the polymer matrix.

Nanotechnology has a wide range of applications in membrane technologies employed in water and wastewater treatment. Many researchers are working on the advancement of antifouling properties of mixed matrix membranes in which nanomaterials are the additives (Escobar 2005, Li *et al*. 2007, 2009, Kim and Bruggen 2010). Nanomaterials are added to the polymer/ polymer matrix for attaining the certain desirable properties which are mentioned below. Specific structures imparted to the polymer matrix consequent to addition of nanomaterials render favourable selectivity and permeability to the membrane for filtration and gas separation in the case of UF and NF membranes. The structure of the membrane matrix can be altered by the addition of nanomaterials and this alters the pore size of the membrane. Thus, a MF membrane can be converted to an UF membrane, and an UF membrane can be altered to a NF membrane. Improvement in the antifouling property of the polymer membranes is another characteristic feature that is achieved by the presence of various functional groups and due to the hydrophilicity of the nanocomposite materials (Li *et al*. 2007, Kim and Bruggen 2010, Roy *et al*. 2011, Razmjou *et al*. 2011, Xu *et al*. 2009). Membranes in which nanoparticles have been incorporated exhibit properties that are considerably different from those of the pristine polymer. These are incorporated by assembling engineered nanoparticles into the porous membranes (Li *et al*. 2009) or blending them with polymeric membranes (Kim *et al*. 2003, Razmjou *et al*. 2011). Inorganic materials like silica, zeolite, graphite, metal oxide nanoparticles, carbon nanotubes, and oxidised multi-walled carbon nanotubes are used as additives in conventional membranes to increase its permeability and fouling-resistance as well as to improve the quality of permeate (Li *et al*. 2009, Merkel *et al*. 2002, Kim *et al*. 2003, Taurozzi *et al*. 2008, Rahimpour *et al*. 2008, Bottino *et al*. 2002).

Researchers have investigated the performance of mixed matrix membranes, fabricated with fMWNTs (Vatanpour *et al*. 2011), GO (Swati *et al*. 2014, Zinadini *et al*. 2014) and

Table 1 Percentage composition of membranes

Psf		NMP		fMWNT/ GO/ MnO_2 NC	
Weight %	Weight (g)	Weight %	Volume (mL)	Weight %	Weight (mg)
15.0	1.50	85	8.5	0.0	0.00
14.5	1.45	85	8.5	0.5	0.05
14.0	1.40	85	8.5	1.0	0.10
12.0	1.20	85	8.5	3.0	0.30

MnO_2 (Jamshidi *et al*. 2014) as additives. The effect of incorporation of this nanocomposite in polysulfone on pure water flux, permeability, porosity, mean pore radius, equilibrium water content, surface morphology, hydrophilicity, antifouling properties and flux recovery have been investigated. In this study, a nanocomposite synthesised from functionalised multi-walled carbon nanotubes (fMWNTs), graphene oxide (GO) and manganese dioxide (MnO_2) nanoparticles (fMWNTs/GO/MnO_2 NC) was used as the additive to fabricate a mixed matrix membrane in which polysulfone is used as the host polymer (Psf/ fMWNTs/GO/ MnO_2 NC membrane).

The main aim of the present work was to investigate the performance of Psf/fMWNTs/GO/MnO_2 NC mixed matrix membrane in the removal of a cationic dye, crystal violet (CV), from aqueous solutions. The structure of crystal violet is presented in Fig. 3. The influence of the concentration of fMWNTs/GO/MnO_2 NC in the polysulfone matrix, initial concentration of the dye, and operating pressure, on the rejection of the dye by the Psf/ fMWNTs/GO/MnO_2 NC mixed matrix membrane was investigated.

2. Materials and methods

Reagent grade chemicals were used in all the experiments. Multi-walled carbon nanotubes (MWNTs, 93%) nitric acid (HNO_3, 70%) and crystal violet (Molecular formula: $C_{25}H_{30}N_3Cl$, Molecular Weight: 408, λ: 580nm) from were procured from Redex Nano Lab, Merck, and SRL respectively. Potassium permanganate ($KMnO_4$), sodium nitrate (KNO_3), hydrogen peroxide (H_2O_2) and sulphuric acid (H_2SO_4) procured from Merck and locally available graphite powder were used for the synthesis of GO. Manganese sulphate monohydrate ($MnSO_4.H_2O$), potassium permanganate ($KMnO_4$, 99.3%), and hydrogen peroxide (H_2O_2, 30%) procured from Merck were used for the synthesis of manganese dioxide (MnO_2) nanoparticles. N - methyl pyrrolidone (NMP) and polysulfone used for membrane fabrication were procured from Sigma Aldrich. Bovine serum albumin (BSA) used in the antifouling analysis was procured from Merck and Potassium bromide (KBr) used in the FTIR spectroscopy from Sigma Aldrich. Distilled water was used for preparation of solutions of different concentrations.

2.1 Synthesis of fMWNTs/GO/MnO_2 nanocomposite

fMWNTs/GO/MnO_2 nanocomposite was prepared by mixing MnO_2, fMWNTs, and GO in equal proportions thoroughly by sonication for 1h in water. After thorough dispersion, the material was dried in ambient air. The dried material was stored for characterisation and fabrication of the Psf/fMWNTs/GO/MnO_2 NC membrane.

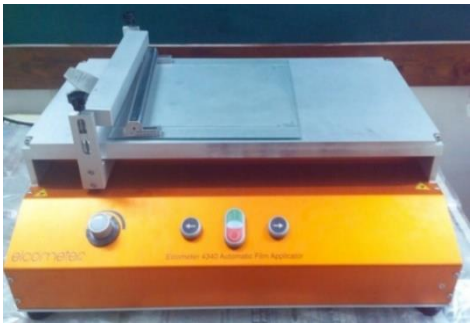

Fig. 4 Motorised film applicator

2.2 Fabrication of Psf/fMWNTs/GO/MnO_2 nanocomposite nanofiltration membranes

The asymmetric, flat sheet type, dense Psf membrane were fabricated by phase inversion induced by the immersion precipitation technique in a non-solvent (water). Pristine Psf membranes and Psf/fMWNTs/GO/MnO_2 NC membranes with fMWNTs/GO/MnO_2 NC as additive were fabricated from a casting solution containing the polymer, polysulfone, and the solvent, NMP.

Table 1 presents the amount of Psf, NMP, and fMWNTs/ GO/MnO_2 NC used in the fabrication of Psf/fMWNTs/GO/ MnO_2 NC membranes with different concentration of fMWNTs/GO/MnO_2 NC. The casting solution was prepared by dissolving Psf in NMP by heating at 60°C in a magnetic stirrer for 12 h. fMWNTs/GO/MnO_2 NC was dispersed in NMP using a sonicator first and then mixed with the Psf-NMP mixture after 8 h of stirring. Stirring continued for about 4h till the formation of a homogeneous mixture of Psf and fMWNTs/GO/MnO_2 NC.

A sonication-assisted method was used for about 10min to remove air bubbles that may be present in the casting solution. Afterwards, the solution was cast onto a clean glass plate using an adjustable (thickness) Baker film applicator (Elcometer, Fig. 4) to obtain a membrane of thickness 200 µm. The glass plate was then immediately immersed into the non-solvent bath of distilled water without any evaporation. After primary phase separation and membrane formation, the membranes were stored in fresh distilled water for 24 h to ensure complete phase separation. Finally, for drying, the membranes were sandwiched between two sheets of filter paper for 24 h at room temperature. The overall scheme of fabrication of the membrane is presented in Fig. 5.

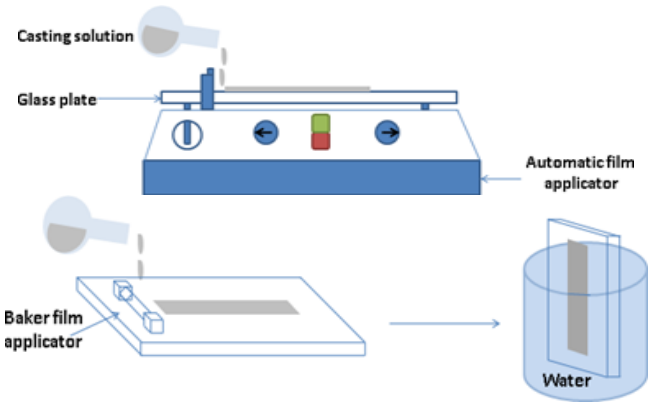

Fig. 5 Overall scheme of fabrication of the membrane

Fig. 6 Cross flow membrane filtration cell (CF042)

3. Characterization

Chemical characterization of the functionalized groups in fMWNTs, GO, and MnO_2 nanoparticles and synthesized nanocomposite-polysulfone membranes was performed by recording its FTIR spectra using a spectrometer (Jasco, 4108). Field Emission Scanning Electron Microscope Hitachi SU6600 was used to analyse the surface morphology of the fMWNT/GO/ MnO_2 NC, Psf, and Psf/ fMWNT/GO/MnO2 NC membranes (with varying amounts of fMWNTs/GO/MnO_2 NC). The membranes were cut into small pieces and cleaned with filter paper. The dried samples were gold sputtered to induce electrical conductivity. Thereafter, these were viewed under an electron microscope at 5kV. Membrane hydrophilicity was assessed in terms of the water contact angle between the membrane surface and water. Water contact angles were measured using the sessile drop method with a goniometer (Digidrop GBX). To minimise experimental errors, this was measured at three random locations for each sample and the average was reported. Other properties of polymer nanocomposite membranes such as equilibrium water content, pure water permeability, mean pore size, and porosity were also determined.

3.1 Equilibrium water content or water uptake

Equilibrium water content or water uptake of the membrane was determined by measuring the difference in weight of the dry membrane, and wet membrane after hydration. The wet weight (w_w) of the membrane was determined after immersing it for 24h in distilled water and then removing the water attached to the surface using a blotting paper. The weight of the dry membrane (w_d) was determined after drying it. The percentage of water uptake was calculated by Eq. (1).

$$Water\ uptake\ \rightleftarrows\ (\%) = \left(\frac{w_w - w_d}{w_d}\right) \times 100 \qquad (1)$$

Table 2 Parameters of the cross flow membrane filtration cell

Parameter	Value
Active Membrane Area	42 cm² (6.5 in²)
Active Area Dimensions	9.207 cm x 4.572 cm
Support Membrane	20 µm sintered stainless steel
Maximum Pressure	69 bar (1000 psig)
Maximum Temperature	80°C (180 °F)
O-ring	Buna-N

3.2 Porosity and pore size of Psf/fMWNTs/GO/MnO_2 NC membrane

Overall porosity (ε) of a membrane is the percentage of volume of pore spaces to the total volume of the membrane. This was determined using gravimetric method (Li *et al.* 2009) using Eq. (2).

$$\varepsilon = \frac{w_w^{w} - w_d}{Ald_w} \times 100 \qquad (2)$$

where, w_w is the weight of the wet membrane; w_d is the weight of the dry membrane; A is the effective area (m^2) of the membrane, d is the density of water (998 kg/m^3) and l is the membrane thickness (m). Mean pore radius (r_m) of the membrane was determined on the basis of the pure water flux, operational pressure, and porosity using the Guerout–Elford–Ferry Eq. (3)

$$r_m = \sqrt{\frac{(2.9 - 1.75\varepsilon) \times 8\eta lQ}{\varepsilon A \Delta P}} \qquad (3)$$

where, η is the viscosity of water (8.9 x 10^{-4}Pa s), Q is the volume of permeated pure water per unit time (m^3/s) and ΔP is the operational pressure.

3.3 Membrane filtration process for the removal of crystal violet

Membrane filtration experiments were performed in a bench-scale membrane filtration system (Sterlitech, USA) with a cross flow cell CF042 (Fig. 6 and Table 2).

The flow diagram of the membrane filtration system is presented in Fig. 7. Feed water was pumped from the feed tank with a high pressure pump to the cross flow cell through the bottom of the filtration cell. The permeate (through the membrane) was collected at the top of the cell; the concentrate flows through the outlet at the bottom to the feed tank. Pressure gauges were provided to measure the pressure in the flow line and valves were used to regulate

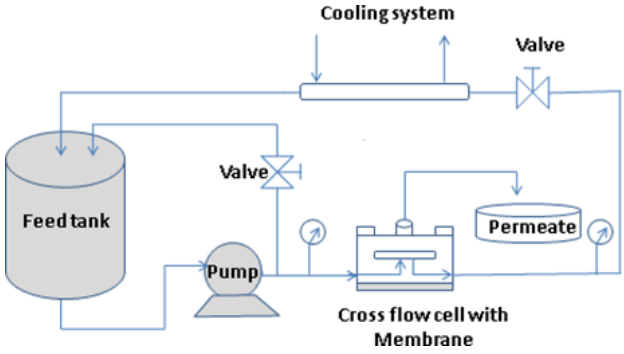

Fig. 7 Flow diagram of membrane filtration

the pressure. A bypass valve was provided to avoid unexpected pressure rise in the system.

3.3.1 Compaction of the membrane

The membrane has to be compacted before any filtration experiment. This enables densification of the inner structure of the membrane so that problems due to compaction during the treatment process can be avoided. It is generally carried out at a pressure 2 to 3 times higher than the highest operating pressure for about 3h with distilled water. In this study, compaction of the membrane was performed at a pressure of 15 bars. The procedure adopted is as follows. The storage tank was filled with distilled water. Connections between the feed tank, pump, cross flow cell and the filtration system were secured and the filtration system was switched on. Distilled water was forced up the membrane using the pump at a pressure of 15 bars. Compaction was continued till the permeate flux, i.e., the volume of water coming out through a unit area of membrane in unit time, became constant. The permeate flux, (kg/m^{2}h) was calculated using Eq. (4).

$$J_w = \frac{m}{A \times \Delta t} \tag{4}$$

where, m is the weight of the permeated pure water (kg), A is effective area of the membrane (m^2) and Δt is the time duration of the permeation experiment (h).

3.3.2 Pure water flux and permeability

After compaction, experiments were performed to determine the pure water flux and pure water permeability of the Psf/fMWNTs/GO/MnO$_2$ NC membranes. Pure water flux of the Psf/fMWNTs/GO/MnO$_2$ NC membranes were determined by pressurizing distilled water through it at different operating pressures ranging from 2 to 8 bars. The quantity of permeate was observed at an interval of 15 min until a steady state is achieved w.r.t. the flux. Pure water flux of the Psf/fMWNTs/GO/MnO$_2$ NC membranes was computed using Eq. (4). Pure water permeability was computed by dividing the pure water flux by the operating pressure (Eq. 5)

$$Pure\ water\ permeability\ (kg/m^2.bar.h) = \frac{J_w}{\Delta P} \tag{5}$$

The performance of the Psf/fMWNTs/GO/MnO$_2$ NC membranes w.r.t. the removal of CV from an aqueous solution of CV dye was evaluated as a function of the concentration of fMWNTs/GO/MnO$_2$ NC in the Psf/fMWNTs/GO/MnO$_2$ NC membranes, operating pressure, and the initial concentration of CV in the aqueous solutions. In all the filtration experiments, the feed tank was filled with an aqueous solution of CV dye and filtration was performed at various pressures until steady state permeate flux was obtained. The permeate was collected every 15min for determining the permeate flux as well as the concentration of CV in it. Percentage rejection of the dye was calculated using Eq. (6).

$$R(\%) = (1 - \frac{C_p}{C_f}) \times 100 \tag{6}$$

where C_p and C_f are the concentrations of CV in the permeate and the feed respectively. Between each of the runs, the membrane was thoroughly washed to remove traces of dye sticking inside the bench-scale membrane filtration unit.

3.3.3 Analysis of membrane fouling

Analysis of membrane fouling was performed with Bovain Serum Albumine (BSA) solution of concentration 150 mg/L at an operating pressure of 5bars. The analysis was performed in three steps. First, the permeate flux with pure water (J_{w1}) was determined. Then, the permeate flux with BSA of concentration 150 mg/L was determined (J_p). After this, the membranes were washed with distilled water and kept immersed in it for about 20 min. This was followed by estimation of pure water flux of the cleaned membranes (J_{w2}). Flux recovery ratio, total fouling ratio, reversible fouling ratio, and irreversible fouling ratio of the Psf and Psf/fMWNTs/GO/MnO$_2$ NC membranes are parameters used to indicate antifouling characteristics of these membranes. Flux recovery ratio (*FRR*) is the ratio of flux obtained for distilled water permeation through the membranes after BSA permeation to that obtained for distilled water permeation through the membranes before BSA permeation. This is expressed in percentage and is calculated by Eq. (7)

$$FR(\%) = \frac{J_{w2}}{J_{w1}} \times 100 \tag{7}$$

High values of *FRR* indicate that the membrane is superior with regard to antifouling properties. In this study, the antifouling properties of the Psf/fMWNTs/GO/MnO$_2$ NC membranes were evaluated by computing the total fouling ratio (R_t), reversible fouling ratio (R_r), and irreversible fouling ratio (R_{ir}). Reversible fouling ratio is a measure of the fouling which can be removed by washing whereas irreversible fouling ratio is related to the fouling which cannot be removed by washing. Total fouling ratio (R_t) is the sum of reversible and irreversible fouling ratios. These parameters were calculated by the following equations.

$$\text{Total fouling ratio} \quad R_t = (1 - \frac{J_p}{J_{w1}}) \times 100 \tag{8}$$

Reversible fouling ratio $R_r = (\frac{J_{w2}-J_p}{J_{w1}}) \times 100$ (9)

Irreversible fouling ratio $R_{ir} = (\frac{J_{w1}-J_{w2}}{J_{w1}}) \times 100$ (10)

4. Results and discussion

4.1 FESEM analysis

The size, shape and structure of the fMWNTs/GO/MnO_2 NC and the surface morphology of the synthesized Psf/ fMWNTs/GO/MnO_2 NC membranes were characterized by imaging with FESEM; the results are presented in Fig. 8.

The structure of the fMWNTs/GO/MnO_2 NC was like spheres of MnO_2 nanoparticles covered by the graphene layers, out of which the fMWNTs spiked out. The FESEM image of the pristine Psf and Psf/fMWNTs/GO/MnO_2 NC membranes exhibited a typical asymmetric structure, and developed macro-voids. Formation of a dense layer on the Psf/fMWNTs/GO/MnO_2 NC membrane could be observed whereas this was absent in the pristine Psf membrane. Fast exchange of solvent and non-solvent in the phase inversion process due to the presence of hydrophilic fMWNTs/GO/ MnO_2 NC in the Psf matrix (Blanco *et al*. 2006), interactions between components in the casting solution, and phase inversion kinetics contributed to this. Through the cracks formed on the surface of the Psf/fMWNTs/ GO/MnO_2 NC membrane, the porous inner structure could be observed.

4.2 FTIR spectra

ATR-FTIR spectroscopy allowed assessing the effectiveness of the hydrogen bonds formed between the fMWNTs/GO/MnO_2 NC in the Psf/fMWNTs/GO/MnO_2 NC membrane and water. Fig. 9 is the FTIR spectra of the Psf and Psf/fMWNTs/GO/MnO_2 NC membranes with 0.1wt% fMWNTs/GO/MnO_2 NC. It exhibited a stretch band at 3400–3600cm^{-1} for the Psf/fMWNTs/GO/MnO_2 NC membrane.

This is the characteristic band of hydrogenation bond and this was absent in the spectra of the pristine Psf membrane. It indicates high affinity of the Psf/fMWNTs/ GO/MnO_2 NC membranes to water.

4.3 Contact angle

Water contact angle of the membranes, determined by the sessile drop method, was used to confirm the conversion of hydrophobic polysulfone membrane to hydrophilic when fMWNTs/GO/MnO_2 NC was incorporated to Psf in varying quantities. From the results, presented in Fig. 10(a), it is observed that the contact angles of the Psf/fMWNTs/GO/ MnO_2 NC membranes gradually decreased from 86.00 to 73.80 when the percentage by weight of fMWNTs/GO/ MnO_2 NC was increased in the mixed matrix membranes from 0 to 0.3%.

This indicated that the hydrophilicity of the membranes

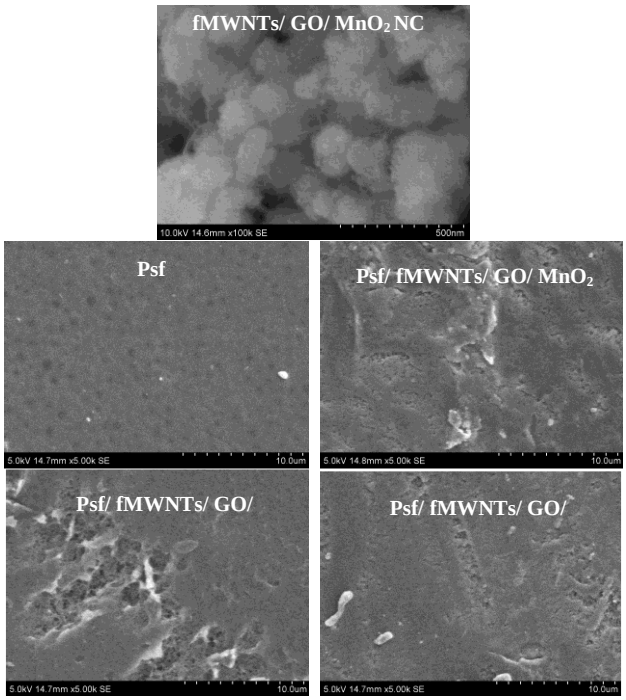

Fig. 8 FESEM image of fMWNTs/GO/MnO_2 NC, pristine Psf, Psf/fMWNTs/GO/MnO_2 NC membranes

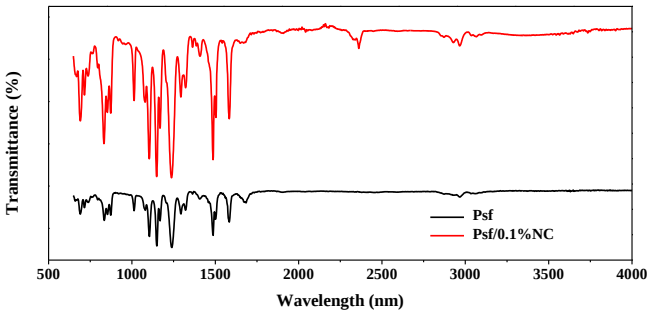

Fig. 9 FTIR spectra of Psf and Psf/fMWNTs/GO/MnO_2 membranes with 0.1wt% fMWNTs/GO/MnO_2

improved with increase in the amount of fMWNTs/GO MnO_2 NC in the Psf/fMWNTs/GO/MnO_2 NC membrane. Decrease in the water contact angle indicates increase in hydrophilicity of the Psf/fMWNTs/GO/MnO_2 NC membranes. This can be explained by the fact that during the phase inversion process, the hydrophilic fMWNTs/GO/ MnO_2 NC migrates spontaneously to the membrane-water interface to reduce the interface energy (Sun *et al*. 2009, Celik *et al*. 2011). By increasing the amount of fMWNTs/ GO/MnO_2 NC in the Psf matrix, the top surface of the membrane, i.e., the surface exposed to water in the phase inversion process, became more hydrophilic than the bottom surface i.e., glass side. This is evident from Fig.10b indicating migration of fMWNTs/GO/MnO_2 NC to the top surface of the membrane. Increasing the amount fMWNTs/ GO/MnO_2 NC to more than 0.1 wt% did not result in further enhancement of hydrophilicity of the Psf/fMWNTs/GO/ MnO_2 NC membranes. Celik *et al*. (2011) also reported a similar behaviour. This might be explained by the irregular positioning of fMWNTs/GO/MnO_2 NC in the membrane structure when the amount of fMWNTs/GO/

MnO_2 NC in the Psf/fMWNTs/GO/MnO_2 NC membrane is higher than 0.1 wt% (Qiu *et al*. 2009), leading to aggregation and reduction in the formation of effective surface with fMWNTs/GO/MnO_2 NC on the Psf/ fMWNTs/ GO/MnO_2 NC membranes. Similar results have been reported by Vatanpour *et al*. (2011). It was also observed that the water contact angle of the Psf/fMWNTs/GO/MnO_2 NC membranes was less for the membrane fabricated by the wet phase inversion process than that for the one fabricated by the dry phase inversion process (Fig. 10(c)). This indicated that the membrane fabricated by wet phase inversion has higher hydrophilicity than that fabricated by dry phase inversion.

4.4 Porosity

Porosity of the fabricated Psf/fMWNTs/GO/MnO_2 NC membranes was calculated using the wet weight and dry weight of the membranes. Variation in the porosity of the Psf/fMWNTs/GO/MnO_2 NC membranes with concentration of fMWNTs/GO/MnO_2 NC in the Psf/fMWNTs/GO/MnO_2 NC membranes is presented in Fig. 11(a). The porosity of the Psf membranes could be greatly enhanced by the inclusion of fMWNTs/GO/MnO_2 NC up to 0.1wt%. This may be due to the fast exchange of NMP with water in the presence of the hydrophilic fMWNTs/GO/MnO_2 NC during the phase inversion process (Blanco *et al*. 2006). When the concentration of fMWNTs/GO/MnO_2 NC was increased to 0.3wt%, porosity started reducing, probably due to reduction in the size of macro-voids. The pore walls form a sub-layer due to pore blocking and increase in viscosity of the Psf/fMWNTs/GO/MnO_2 NC blend solution due to the inclusion of fMWNTs/GO/MnO_2 NC (Han and Nam 2002, Vatanpour *et al*. 2011).

The two factors affecting porosity of the membranes are the hydrophilicity of the membrane and the viscosity of the membrane casting solution. Hydrophilicity plays a role in increasing the porosity of the membrane upto 0.1wt% concentration of fMWNTs/GO/MnO_2 NC in the Psf/ fMWNTs/GO/MnO_2 NC membranes. When the concentration of fMWNTs/GO/MnO_2 NC exceeds 0.1wt%, viscosity of the casting solution hinders the exchange between the solvent and the non-solvent during phase inversion, slows down the precipitation of the membrane, causes clustering of the fMWNTs/GO/MnO_2 NC during phase inversion and suppresses the porous structure inside the membrane (Wu *et al*. 2010). Therefore, a less porous membrane is created. The flux decreased in the case of the Psf/fMWNTs/GO/MnO_2 NC membrane with 0.3wt% of fMWNTs/GO/MnO_2 NC. A similar behaviour was observed by Vatanpour *et al*. (2011) with MWNT/PES NF membranes, Wu *et al*. (2010) in carboxylated MWNT/ brominated polyphenylene oxide (BPPO) UF membranes and Choi *et al*. (2007) in oxidized MWNT/Psf membranes.

4.5 Equilibrium water content

Equilibrium water content of Psf/fMWNTs/GO/MnO_2 NC membranes with different concentrations of fMWNTs/ GO/MnO_2 NC was determined by measuring the difference in weight of the dry membrane and wet membrane after

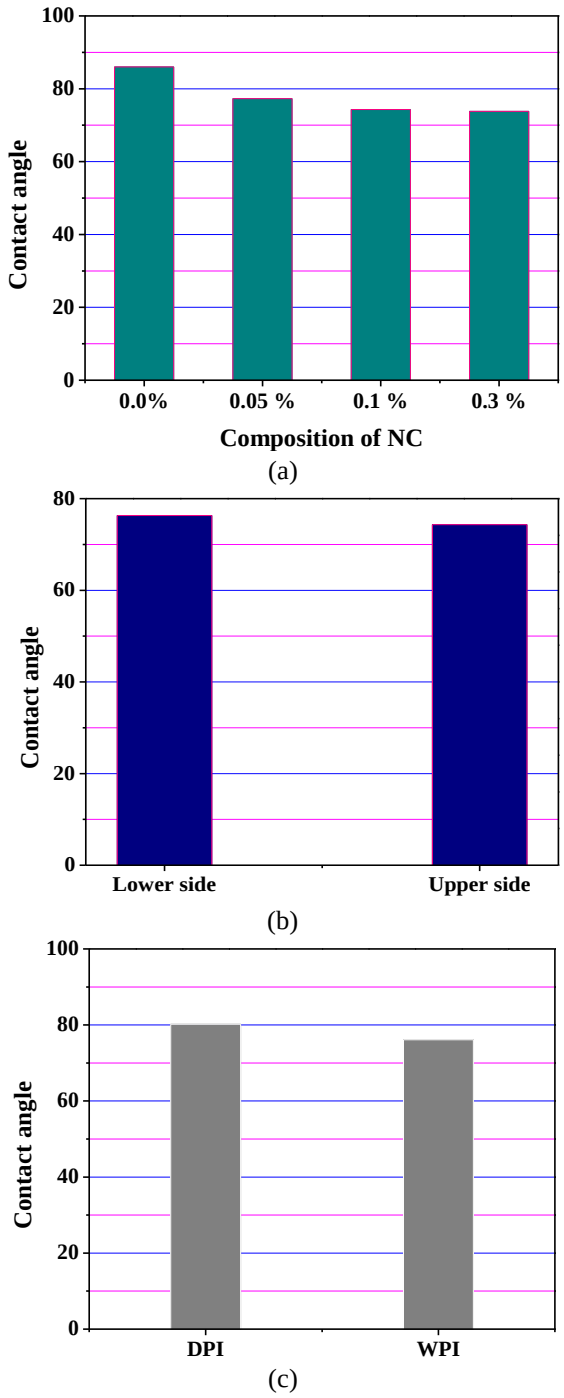

Fig. 10 Variation of contact angle with a) concentration of fMWNTs/GO/MnO_2 NC in Psf/fMWNTs/GO/MnO_2 NC membranes, b) upper and lower side of Psf/ fMWNTs/GO/MnO_2 NC membrane and c) type of phase inversion process

hydration. The results presented in Fig. 11(a) indicate that there is huge improvement in the equilibrium water content of the membrane when fMWNTs/GO/MnO_2 NC was incorporated into the pristine Psf membrane. This may be due to the incorporation of hydrophilic fMWNTs/GO/MnO_2 NC, which can absorb more water into the membranes (Vatanpour *et al*. 2011).

It was also observed that the membrane with 0.1wt%

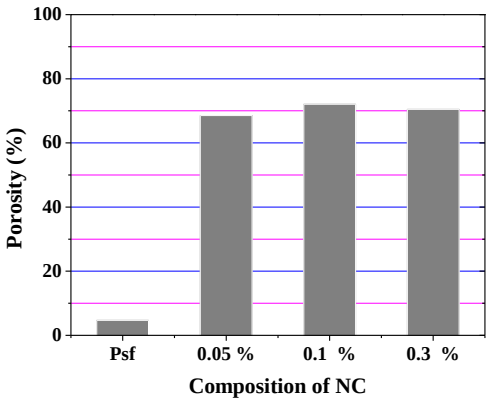

(a)

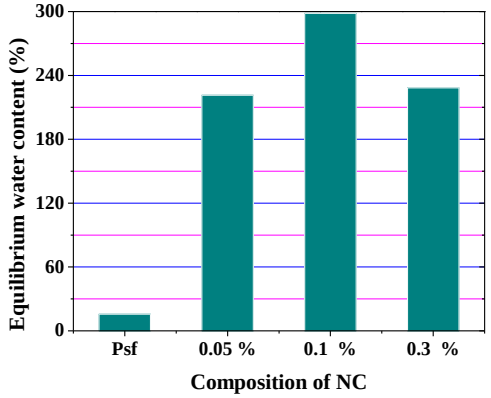

(b)

Fig. 11 Effect of concentration of fMWNTs/GO/MnO_2 NC in Psf/fMWNTs/GO/MnO_2 NC membranes on (a) Porosity and (b) equilibrium water content of Psf/ fMWNTs/ GO/ MnO_2 NC membranes

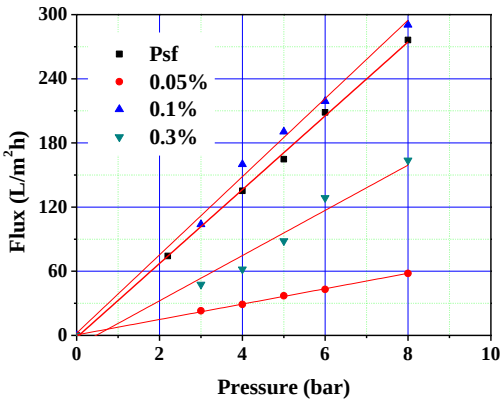

(a)

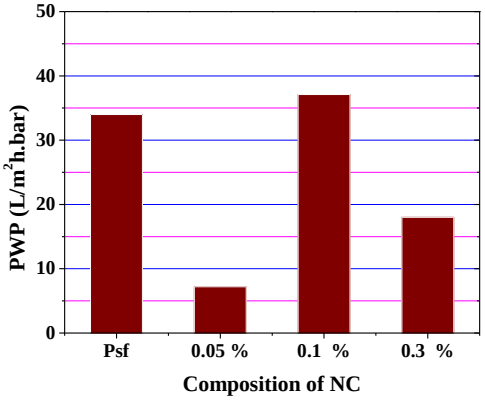

(b)

Fig. 12 Effect of (a) operating pressure on pure water flux and (b) concentration of fMWNTs/GO/MnO_2 NC in Psf/fMWNTs/GO/MnO_2 NC membranes on pure water permeability

fMWNTs/GO/MnO_2 NC in Psf exhibited the highest equilibrium water content. Psf/fMWNTs/GO/MnO_2 NC membranes with 0.05wt% fMWNTs/GO/MnO_2 NC exhibited relatively low equilibrium water content because it contained lesser amount of the fMWNTs/GO/MnO_2 NC. The Psf/fMWNTs/GO/MnO_2 NC membrane containing .3wt% fMWNTs/GO/MnO_2 NC exhibited a relatively lower equilibrium water content because of the agglomeration of fMWNTs/GO/MnO_2 NC which hindered the absorption of water molecules.

4.6 Pure water flux and permeability

Pure water flux and permeability of the Psf/fMWNTs/ GO/MnO_2 NC membranes were determined by pressurizing distilled water through the membranes at an operating pressure ranging from 2 to 8 bars. The pure water flux and permeability of the Psf/fMWNTs/GO/MnO_2 NC membranes with different concentrations of the nanocomposite as well as that of the pristine Psf membrane are presented in Figs.12a and 12b respectively. Pure water flux increased with increase in operating pressure because the force pushing water through the membranes increases with increase in operating pressure.

Pure water permeability of the Psf/fMWNTs/GO/MnO_2 NC membranes increased when the concentration of fMWNTs/ GO/MnO_2 NC in the membrane was increased from 0.05wt% to 0.1wt%. Thereafter, it exhibited a decline when the concentration of the fMWNTs/GO/MnO_2 NC was increased to 0.3wt%.

Hydrophilicity and pore size are the two factors that control permeation of pure water through the membranes. As already mentioned, the hydrophilic fMWNTs/GO/MnO_2 NC in the top layer of the Psf/fMWNTs/GO/MnO_2 NC membranes improves the hydrophilicity of the membrane surface, resulting in an increase in pure water flux. An increase in pore size also leads to enhanced permeation of water through the membranes. Enhancement in pure water flux up to 0.1wt% of fMWNTs/GO/MnO_2 NC in the membrane may be attributed to improvement of membrane hydrophilicity and increase in pore size of the top-layer, caused by increase in the exchange rate of solvent to non-solvent during formation of the Psf/fMWNTs/GO/ MnO_2 NC membranes in the phase inversion process.

4.7 Mean pore radius

Mean pore radius of the fabricated membranes with different concentrations of fMWNTs/GO/MnO_2 NC was calculated using the Grout–Alford–Ferry equation, using the known values of porosity, effective area and thickness of the membranes, and flow rate at a particular operating

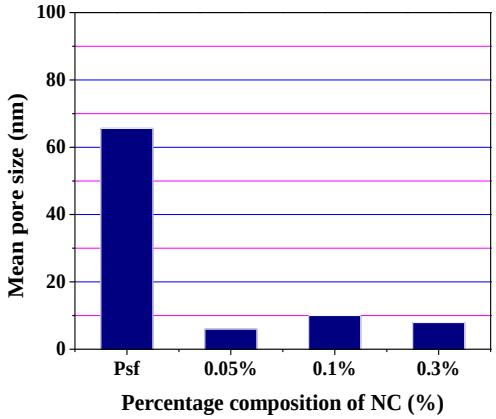

Fig. 13 Effect of concentration of fMWNTs/GO/MnO_2 NC in Psf/ fMWNTs/GO/MnO_2 NC membranes on mean pore radius of the membranes

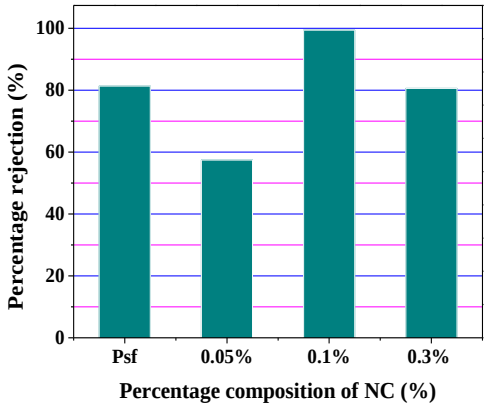

Fig. 14 Effect of concentration of fMWNTs/GO/MnO_2 NC in the Psf matrix on rejection of CV by Psf/ fMWNTs/GO/ MnO_2 NC membranes

pressure. From the results presented in Fig. 13, it is observed that the size of the pores in the pristine Psf membrane was in the range of that of UF membranes. But when fMWNTs/GO/ MnO_2 NC was incorporated into the pristine Psf membrane, the mean pore size reduced to the range of NF membranes. This is because as fMWNTs/ GO/MnO_2 NC is added to pristine Psf, the viscosity of the casting solution increases. This, in turn, reduces the mean pore radius of the membrane (Wu *et al*. 2010) and causes a decrease in water flux. Incorporation of fMWNTs/GO/ MnO_2 NC can also cause blocking of the pores.

4.8 Membrane filtration experiments

The capability of nanofiltration membranes to separate CV dye from aqueous solution was assessed by performing membrane filtration experiments with CV solutions of various concentrations ranging from 0.5 to 10mg/L. The effect of operating pressure on the removal of CV by filtration through the Psf/fMWNTs/GO/MnO_2 NC membrane was also investigated. The antifouling characteristics of the Psf/fMWNTs/GO/MnO_2 NC membrane with 0.1wt% of the nanocomposite was compared with that of pristine Psf membrane.

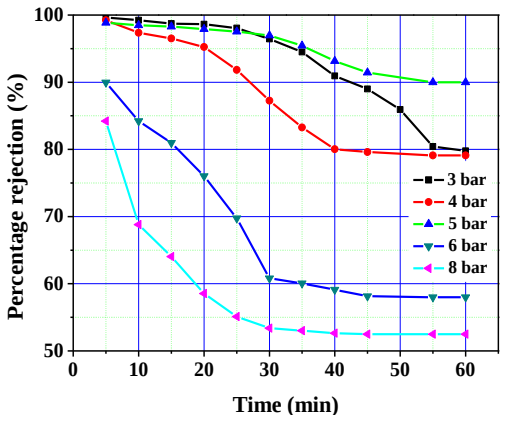

(a)

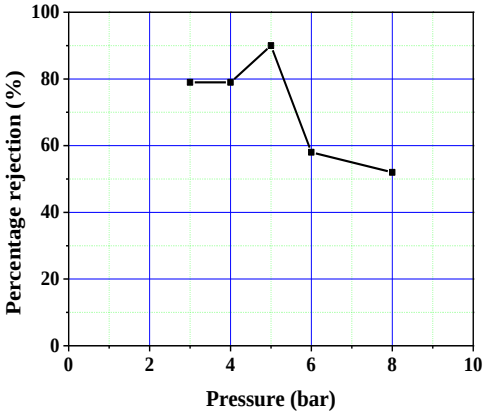

(b)

Fig. 15 Effect of (a) time and (b) operating pressure on the rejection of CV by Psf/fMWNTs/GO/MnO_2 NC membrane with 0.1wt% fMWNTs/GO/MnO_2 NC

4.8.1 Effect of concentration of fMWNTs/GO/MnO_2 NC in Psf/fMWNTs/GO/MnO_2 NC membranes on rejection of CV

The effect of concentration of fMWNTs/GO/MnO_2 NC in the Psf/fMWNTs/GO/MnO_2 NC membranes on the removal of CV from aqueous solution by membrane filtration was investigated at a constant operating pressure of 5 bars. From the results of the study presented in Fig. 14, it is observed that the highest removal was obtained for the Psf/ fMWNTs/GO/MnO_2 NC membrane with 0.1wt% of fMWNTs/GO/MnO_2 NC. The percentage removal observed at different concentrations of the fMWNTs/GO/MnO_2 NC in the Psf membrane exhibited a trend similar to that observed in the case of pure water permeability of the membrane. This can be due to the overall effect of all the properties of the membrane such as porosity, equilibrium water content, and hydrophilicity. It can be concluded that 0.1wt% of fMWNTs/GO/MnO_2 NC in Psf is the optimum concentration for maximum removal of CV from aqueous solution by membrane filtration. All further investigations on the rejection of CV with membranes were performed on Psf/fMWNTs/GO/MnO_2 NC membranes with 0.1wt% of fMWNTs/ GO/MnO_2 NC.

4.8.2 Effect of operating pressure on percentage rejection of CV from aqueous solutions

The observed removal of CV from aqueous solution by

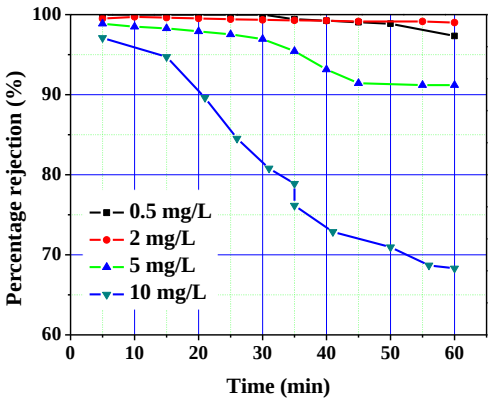

Fig. 16 Effect of initial concentration of aqueous solution of CV on percentage rejection by Psf/fMWNTs/GO/MnO_2 NC membrane

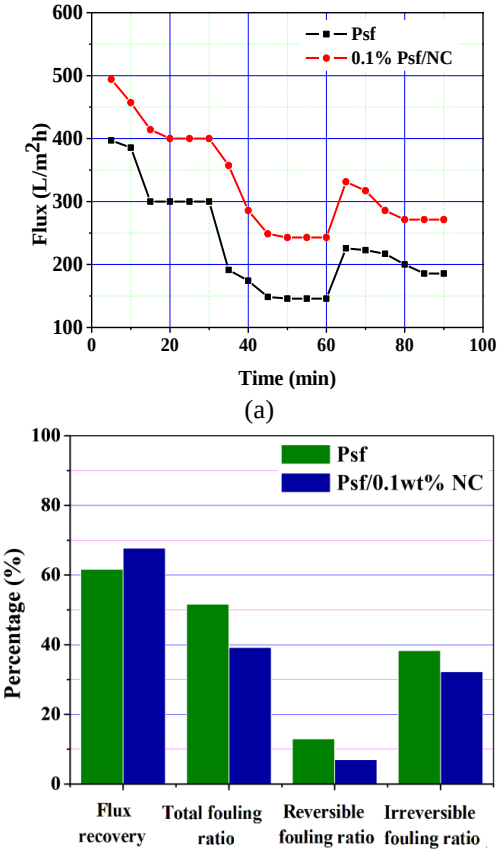

Fig. 17 (a) Flux versus time - Analysis of antifouling and (b) comparison of flux recovery and fouling ratio of Psf and Psf/fMWNTs/GO/MnO_2 NC membrane with 0.1wt% fMWNTs/GO/MnO_2 NC

the Psf/fMWNTs/GO/MnO_2 NC membrane with 0.1wt% of the nanocomposite at various operating pressures is presented in Fig. 15(a). Removal increased with time and finally attained a steady state value at all the operating pressures.

The time required to attain a steady removal varied with the operating pressure. At higher operating pressures, the time required for attaining steady state was less than that at lower operating pressures. The increase in observed removal was found to be very high in the beginning. This is because the dye molecules rejected by the Psf/fMWNTs/GO/MnO_2 NC membrane accumulates on the surface of the membrane in the beginning, hindering the passage of other dye molecules. However, increase in percentage removal considerably slows down with time; this may be due to concentration polarization. Since the effect of concentration polarization increases, concentration of the dye at the surface of the membrane increases with time. The net difference between the concentration of the dye in the feed and the permeate increases.

This increase in the concentration gradient acts as the driving force to cause more and more dye molecules to flow through the membrane, thereby resulting in increased concentration of CV in the permeate. It was observed that the observed removal was the maximum at an operating pressure of 5 bar (Fig. 15(b)). This may be due to lower effect of concentration polarisation at this pressure. Thus the operating pressure of 5 bars can be treated as the optimum for the removal of CV from an aqueous solution using a Psf/fMWNTs/GO/MnO_2 NC membrane with 0.1wt% of the nanocomposite.

4.8.3 Effect of initial concentration

The effect of initial concentration of CV on the percentage removal of CV by the Psf/fMWNTs/GO/MnO_2 NC membrane with 0.1wt% fMWNTs/GO/MnO_2 NC was investigated using aqueous solutions with different concentrations of CV – 0.5 mg/L, 2 mg/L, 5 mg/L and 10 mg/L - at an operating pressure of 5bars. From the results presented in Fig. 16, it is observed that almost 100% removal was obtained from the aqueous solutions with concentrations 0.5 mg/L and 2 mg/L of CV. Removal of CV from the aqueous solutions with concentrations 5 mg/L and 10 mg/L was 92% and 68% respectively.

4.8.4 Analysis of antifouling

Analysis of antifouling properties of pristine Psf membrane and Psf/fMWNTs/GO/MnO_2 NC membranes with 0.1wt% fMWNTs/GO/MnO_2 NC was performed by measuring water flux recovery after fouling by Bovine Serum Albumine (BSA) solution (concentration of aqueous dolution of CV = 150 mg/L). From the results of the analysis presented in Fig. 17(a), it is observed that the flux recovery ratio (FRR) of the Psf/fMWNTs/GO/MnO_2 NC membranes with 0.1wt% fMWNTs/GO/MnO_2 NC was higher than that of the pristine Psf membrane. This indicated that the antifouling property of the pristine Psf membrane could be enhanced by incorporating fMWNTs/GO/MnO_2 NC into the Psf matrix. Four types of forces are responsible for the adsorption of proteins onto solid surfaces from aqueous solution, namely, electrostatic force, hydrogen bonding force, hydrophobic force, and Van der Waals force (Déjardin 2006). The isoelectric point of BSA is about 4.9 (Boributh *et al.* 2009), and pH value of the BSA solution is 7. Therefore, BSA molecules are negatively charged in this condition. The functionalized groups such as fMWNTs/GO/MnO_2 NC, that existed on the surface of the membranes were also negatively charged at pH 7 due to dissociation. The strong electrostatic repulsion force between the negatively charged BSA molecules and the

membrane surface is an important reason for improvement in the antifouling performance (Boributh *et al*. 2009, Huisman *et al*. 2000). Membrane fouling is primarily caused by the adsorption and deposition of proteins on the membrane surface and entrapment of proteins in the pores. Due to the relatively high hydrophilicity of the Psf/ fMWNTs/GO/MnO_2 NC membrane with 0.1wt% fMWNTs/ GO/MnO_2 NC, a layer of water is adsorbed. This prevents adsorption of protein on the surfaces of the membranes and enhances the antifouling properties of the Psf/fMWNTs/ GO/MnO_2 NC membranes. Membrane fouling consists of reversible fouling and irreversible fouling. The sum of reversible fouling and irreversible fouling is the total fouling. Reversible fouling can be removed by simple hydraulic cleaning. On the contrary, irreversible fouling is caused by firm adsorption of protein molecules on the surface or entrapment of protein molecules in the pores (Peng *et al*. 2011, Pieracci *et al*. 2002). Fig. 17(a) presents the results of analysis of antifouling of the pristine Psf membrane and the Psf/fMWNTs/GO/MnO_2 NC membranes with 0.1wt% fMWNTs/GO/MnO_2 NC in three steps. The first stage is the permeation of pure water through the membranes for a duration of 30min. Flux obtained in this stage was about 300 L/m^2h and 400 L/m^2h for pristine the Psf membrane and the Psf/fMWNTs/GO/MnO_2 NC membrane respectively. The flux obtained in the second stage (permeation of the solution of BSA through the membranes) was 150 L/m^2h and 250 L/m^2h for the pristine Psf membrane and the Psf/fMWNTs/GO/MnO_2 NC membrane respectively. In the third stage (permeation of pure water through the membranes), the flux obtained was 185 L/m^2h and 271 L/m^2h for the pristine Psf membrane and the Psf/fMWNTs/GO/MnO_2 NC membrane respectively. Results of reversible fouling, irreversible fouling, and total fouling ratios are presented in Fig. 17(b).

From the Fig. 17 (b), it is observed that the total fouling ratio of the pristine Psf membrane was higher than that of Psf/fMWNTs/GO/MnO_2 NC membrane with 0.1wt% fMWNTs/GO/MnO_2 NC by 12%. The difference between the irreversible fouling resistance of the Psf and the Psf/ fMWNTs/GO/MnO_2 NC membranes with 0.1wt% fMWNTs/ GO/MnO_2 NC was observed to be higher than the difference between the reversible fouling resistance of these membranes. This implies that irreversible fouling dominates total fouling. The pristine Psf membrane exhibited higher irreversible fouling ratio than the Psf/fMWNTs/GO/MnO_2 NC membrane with 0.1wt% fMWNTs/GO/MnO_2 NC due to the relatively lower hydrophilicity and surface charge imparted by the fMWNTs/ GO/MnO_2 NC.

5. Conclusions

A polymer nanocomposite membrane was synthesised by dispersing fMWNTs/GO/MnO_2 NC in polysulfone matrix. fMWNTs/GO/MnO_2 NC was synthesised by sonicating fMWNTs, GO and MnO_2 in equal proportions. Incorporation of fMWNTs/GO/MnO_2 NC in polysulfone resulted in an increase in hydrophilicity, as indicated by a comparison of the values of water contact angle, equilibrium water content, pure water flux, and pure water permeability of this membrane and the corresponding values for the pristine Psf membrane. The values of these characteristics were the maximum for the Psf/fMWNTs/ GO/MnO_2 NC membrane with 0.1wt% of the nanocomposite. Incorporation of fMWNTs/GO/MnO_2 NC in the polysulfone matrix also altered the mean pore size and porosity of the pristine Psf membrane. Percentage rejection of CV was the highest for the Psf/fMWNTs/GO/MnO_2 NC membrane with 0.1wt% of the nanocomposite. The optimum operating pressure, corresponding to which the maximum removal of CV was observed from the aqueous solutions was 5 bars. Almost 100% removal of CV was obtained from the aqueous solutions with initial concentration of CV up to 2 mg/L. Incorporation of fMWNTs/GO/MnO_2 NC in the Psf matrix resulted in an increase in the recovery ratio and decrease in the total fouling ratio of the membrane when compared to the pristine Psf membrane.

Acknowledgment

The financial support to the first author by the University Grants Commission (UGC) (Grant Number F.2-11/2009 (SA-1)), Govt. of India, is also gratefully acknowledged.

References

Blanco, J.F., Sublet, J., Nguyen, Q.T. and Schaetzel, P. (2006), "Formation and morphology studies of different polysulfones-based membranes made by wet phase inversion process", *J. Membr. Sci.*, **283**(1-2), 27-37. https://doi.org/10.1016/j.memsci.2006.06.011.

Boributh, S., Chanachai, A. and Jiraratananon, R. (2009), "Modification of PVDF membrane by chitosan solution for reducing protein fouling", *J. Membr. Sci.*, **342**(1-2), 97-104. https://doi.org/10.1016/j.memsci.2009.06.022.

Bottino, A., Capannelli, G. and Comite, A. (2002), "Preparation and characterization of novel porous PVDF-ZrO_2 composite membranes", *Desalination*, **146**(1-3), 35-40. https://doi.org/10.1016/S0011-9164(02)00469-1.

Choi, J.H., Jegal, J. and Kim, W.N. (2007), "Modification of performances of various membranes using MWNTs as a modifier" *Macromol. Symp.*, **1**(1), 249-250. https://doi.org/10.1002/masy.200750444.

Déjardin, P. (2006), *Proteins at Solid-Liquid Interfaces*, Springer-Verlag, Berlin, Germany.

Escobar, I. (2005), "Committee report: Recent advances and research needs in membrane fouling", *J. Am. Water Works Ass.*, **97**(8), 79-89. https://doi.org/10.1002/j.1551-8833.2005.tb07452.x.

Evrim, C., Park, H. and Choi, H. (2011), "Carbon nanotube blended polyethersulfone membranes for fouling control in water treatment", *Water Res.*, **45**(1), 274-282. https://doi.org/10.1016/j.watres.2010.07.060.

Gohari, R.J., Halakoo, E., Lau, W.J., Kassim, M.A., Matsuura, T. and Ismail, A.F. (2014), "Novel polyethersulfone (PES)/ hydrous manganese dioxide (HMO) mixed matrix membranes with improved anti-fouling properties for oily wastewater treatment process", *RSC Adv.*, **4**(34), 17587-17596. https://doi.org/10.1039/C4RA00032C.

Gryta, M. (2010), "Application of membrane distillation process

for tap water purification", *Membr. Water Treat.*, **1**(1), 1-12. https://doi.org/10.12989/mwt.2010.1.1.001.

Han M.J. and Nam, S.T. (2002), "Thermodynamic and rheological variation in polysulfone solution by PVP and its effect in the preparation of phase inversion membrane", *J. Membr. Sci.*, **202**(1-2), 55-61. https://doi.org/10.1016/S0376-7388(01)00718-9.

Higuchi, A., Tamai, M., Tagawa, Y., Chang, Y. and Ling, Q.D. (2010), "Surface modification of polymeric membranes for low protein binding", *Membr. Water Treat.*, **1**(2), 103-120. https://doi.org/10.12989/mwt.2010.1.2.103.

Huisman, I.H., Prádanos, P. and Hernández, A. (2000), "The effect of protein-protein and protein-membrane interactions on membrane fouling in ultrafiltration", *J. Membr. Sci.*, **179**(1-2), 79-90. https://doi.org/10.1016/S0376-7388(00)00501-9.

Julian, S.T., Hari, A., Volodymyr, Z.B., Anatoliy, F.B., Thomas, C.V., Merlin, L.B. and Volodymyr, V.T. (2008), "Effect of filler incorporation route on the properties of polysulfone- silver nanocomposite membranes of different porosities", *J. Membr. Sci.*, **325**(1), 58-68. https://doi.org/10.1016/j.memsci.2008.07.010.

Kim J. and Van der Bruggen, B. (2010), "The use of nanoparticles in polymeric and ceramic membrane structures: Review of manufacturing procedures and performance improvement for water treatment", *Environ Pollut.*, **158**(7), 2335-2349. https://doi.org/10.1016/j.envpol.2010.03.024.

Kim, S.H., Kwak, S.Y., Sohn, B.H. and Park, T.H. (2003), "Design of TiO_2 nanoparticle self-assembled aromatic polyamide thin-film-composite (TFC) membrane as an approach to solve biofouling problem", *J. Membr. Sci.*, **211**(1), 157-165. https://doi.org/10.1016/j.envpol.2010.03.024.

Ladan, E., Mokhtar, A., and Elmira, P. (2014), "Evaluation of Adsorption characteristics of multiwalled carbon nanotubes modified by a poly(propylene imine) dendrimer in single and multiple dye solutions: Isotherms, kinetics, and thermo-dynamics", *J. Chem. Eng. Data*, **375**(1), 1-2. https://doi.org/10.1021/je400913z.

Li, J.B., Zhu, J.W. and Zheng, M.S. (2007), "Morphologies and properties of poly(phthalazinone ether sulfone ketone) matrix ultrafiltration membranes with entrapped TiO_2 nanoparticles", *J. Appl. Polym. Sci.*, **103**(6), 3623-3629.

Li, J.F., Xu, Z.L., Yang, H., Yu, L.Y. and Liu, M. (2009), "Effect ofTiO_2 nanoparticles on the surface morphology and performance of microporous PES membrane", *Appl. Surf. Sci.*, **255**(9), 4725-4732.

Maskan, F., Wiley, D.E., Johnston, L.P.M. and Clements, D.J. (2000), "Optimal design of reverse osmosis module networks", *AIChE J.*, **46s**(5), 946-954. https://doi.org/10.1002/aic.690460509.

Merkel, T.C., Freeman, B.D., Spontak, R.J., He, Z., Pinnau, I., Meakin, P. and Hill, A.J. (2002) "Ultrapermeable, reverse-selective nanocomposite membranes", *Science*, **296**(5567), 519-522. https://doi.org/10.1126/science.1069580.

Morao, A.I.C., Szymczyk, A., Fievet, P. and Alves, A.M.B. (2010), "Nanofiltration of multi-ionic solutions: Prediction of ions transport using the SEDE model", *Membr. Water Treat.*, **1**(2), 139-158. https://doi.org/10.12989/mwt.2010.1.2.139.

Nandi, B.K., Das, B., Uppaluri, R., Purkait, M.K. (2010), "Preparation and characterization of inexpensive submicron range inorganic microfiltration membranes", *Membr. Water Treat.*, **1**(2), 121-137. https://doi.org/10.12989/mwt.2010.1.2.121.

Peng, J., Su, Y., Shi, Q., Chen, W. and Jiang, Z. (2011), "Protein fouling resistant membrane prepared by amphiphilic pegylated polyethersulfone", *Bioresource. Technol.*, **102**(3), 2289-2295. https://doi.org/10.1016/j.biortech.2010.10.045.

Pieracci, J., Crivello, J.V. and Belfort, G. (2002), "Increasing membrane permeability of UV-modified poly(ether sulfone) ultrafiltration membranes", *J. Membr. Sci.*, **202(**1-2), 1-16. https://doi.org/10.1016/S0376-7388(01)00624-X.

Qiu, S., Wu, L., Pan, X., Zhang, L., Chen, H. and Gao, C. (2009), "Preparation and properties of functionalized carbon nanotube/ PSF blend ultrafiltration membranes", *J. Membr. Sci.*, **342**(1-2), 165-172. https://doi.org/10.1016/j.memsci.2009.06.041.

Rahimpour, A., Madaeni, S.S., Taheri, A.H. and Mansourpanah, Y. (2008), "Coupling TiO_2 nanoparticles with UV irradiation for modification of polyethersulfone ultrafiltration membranes", *J. Membr. Sci.*, **313**(1-2), 158-169. https://doi.org/10.1016/j.memsci.2007.12.075.

Razmjou, A., Mansouri, J. and Chen, V. (2011), "The effects of mechanical and chemical modification of TiO_2 nanoparticles on the surface chemistry, structure and fouling performance of PES ultrafiltration membranes", *J. Membr. Sci.*, **378** (1-2), 73-84. https://doi.org/10.1016/j.memsci.2010.10.019.

Roy, S., Ntim, S.A., Mitra, S. and Sirkar, K.K. (2011), "Facile fabrication of superior nanofiltration membranes from interfacially polymerized CNT-polymer composites", *J. Membr. Sci.*, **375**(1-2), 81-87. https://doi.org/10.1016/j.memsci.2011.03.012.

Sablani, S., Goosen, M., Al-Belushi, R. and Wilf, M. (2001), "Concentration polarization in ultrafiltration and reverse osmosis: A critical review", *Desalination*, **141**(3), 269-289. https://doi.org/10.1016/S0011-9164(01)85005-0.

Swati, G., Prem, P.S., Hariom, G., Vaibhav, K. and Prafulla, K.J. (2014), "Preparation of graphene oxide nano-composite ion-exchange membranes for desalination application", *RSC Adv.*, **4**, 24662-24670. https://doi.org/10.1039/C4RA02216E.

Tanaka, Y. (2010), "A computer simulation of ion exchange membrane electrodialysis for concentration of seawater", *Membr. Water Treat.*, **1**(1), 13-37. http://doi.org/10.12989/mwt.2010.1.1.013.

Vatanpour, V., Madaeni, S.S., Moradian, R., Zinadini, S. and Astinchap, B. (2011), "Fabrication and characterization of novel antifouling nanofiltration membrane prepared from oxidized multiwalled carbon nanotube/polyethersulfone nanocomposite", *J. Membr. Sci.*, **375**(1-2), 284-294. https://doi.org/10.1016/j.memsci.2011.03.055.

Wang, F. and Tarabara, V.V. (2007), "Coupled effects of colloidal deposition and salt concentration polarization on reverse osmosis membrane performance", *J. Membr. Sci*., **293**(1-2), 111-123. https://doi.org/10.1016/j.memsci.2007.02.003.

Wu, H., Tang, B. and Wu, P. (2010), "Novel ultrafiltration membranes prepared from a multi-walled carbon nanotubes/ polymer composite", *J. Membr. Sci.*, **362**(1-2), 374-383. https://doi.org/10.1016/j.memsci.2010.06.064.

Xu, Z., Yu, L. and Han, L. (2009), "Polymer-nanoinorganic particles composite membranes: A brief overview", *Front. Chem. Eng. China*., **3**(3), 318-329. https://doi.org/10.1007/s11705-009-0199-0.

Zinadini, S., Zinatizadeh, A.A., Rahimi, M., Vatanpour, V. and Zangeneh, H. (2011), "Preparation of a novel antifouling mixed matrix PES membrane by embedding graphene oxide nanoplates", *J. Membr. Sci.*, **453**, 292-301. https://doi.org/10.1016/j.memsci.2013.10.070.

CC